Available online at www.sciencedirect.com
ScienceDirect
Renewable and Sustainable Energy Reviews
11 (2007) 1087–1116
RENEWABLE & SUSTAINABLE ENERGY REVIEWS
www.elsevier.com/locate/rser

Experimental and CFD investigation of an ICSSWH at various inclinations

D. Henderson*, H. Junaidi, T. Muneer, T. Grassie, J. Currie

Applied Energy Research Group, Napier University, 10 Colinton Road, Edinburgh EH10 5DT, UK

Received 29 September 2005; accepted 23 November 2005

Abstract

The integrated collector storage (ICS) is the type of solar water heater that has retained its existance for well over a century. The flat absorber plate ICS collector type is a relatively recent addition. Being effective, low cost and simple to manufacture, their importance has been further enhanced by the recent upsurge in efforts to effectively tap renewable energy resources. Having different inclinations based on latitude, the design of flat plate heaters can benefit from extensive amount of research on the topic of natural convection in inclined cavities. More than half-century of exploration on inclined cavities has witnessed added activity particularly in the last three decades. Despite this consistent research, efforts to apply the outcomes to the flat plate collectors have been few and collectors reported in the literature appear to be deficient in embedding the knowledge into the design parameters. For an ICS type heater, natural convection studies gain even more weight as the apparatus is functionally an assembly of two natural convection cavities: an air cavity (space between the absorber and cover plates) and a water cavity (water storage tank). An extensive review of previous studies on inclined cavities relevant to flat plate collectors has been complied and discussed. Experimental tests of the ICS heater have been conducted for controlled heat flux up to 400 W. The thermal performance of the heater is recorded experimentally at angles 0–60° from horizontal, in 15° intervals. CFD analysis is also carried out for the same and is found to be in good agreement with previous studies. It was found that for any given constant value of heat flux, the performance of the heater is a strong function of the angle of inclination. The optimum configuration of the heater for Edinburgh conditions (latitude 55°55′N) is also evaluated. The present study also covers the convective behavior inside the water tank, which has been neglected in the past. A step-by-step build-up approach is adopted to resolve water tank behavior as its treatment as a simple natural

*Corresponding author. Tel.: +44 131 455 2324; fax: +44 131 455 2264.
E-mail address: d.henderson@napier.ac.uk (D. Henderson).

doi:10.1016/j.rser.2005.11.003

Nomenclature

$Ra = \frac{g\beta(T_{ap}-T_{gc})L^3}{v\alpha}$	
$Nu = \frac{hx}{k}$	
$Pr = \frac{v}{\alpha} = \frac{C_p\mu}{k}$	
Φ	angle of inclination of cavity
Θ	angle of inclination of heater
h	convective heat transfer coefficient (W/m^2 °C)
x	thickness of the cavity, characteristic length (m)
k	thermal conductivity (W/m °C)
v	kinematic viscosity (m^2/s)
α	thermal diffusivity (m^2/s)
β	thermal expansion (1/°C)
ρ	density (kg/m^3)
L	characteristic length/cavity thickness (m)
U	X-velocity (m/s)
V	Y-velocity (m/s)
T_P	absorber plate temperature (°C)
T_C	glass cover temperature (°C)
T_a	ambient temperature (°C)
A	vertical aspect ratio (H/L)
A_H	horizontal aspect ratio (W/L)
g	acceleration of gravity (m/s^2)
h_o	enthalpy (J)
Nu	Nusselt number
Ra	Rayleigh number
Gr	Grashof number
MBD	mean bias difference
RMSD	root mean square difference

convention cavity is invalid. This article would serve as a design guide for developing heaters tailored for a specific geographical location.

Keywords: Renewable energy; Natural convection; Inclined cavity; Solar water heating; Computational fluid dynamics; ICSSWH

Contents

1. Introduction

Natural convection in inclined cavities or rectangular enclosures has been a topic of widespread interest, and an exhaustive amount of research. The key application of this study is the built-in storage solar water heater, more commonly known as an integrated collector storage (ICS) heater.

The ICS heaters are a popular, inexpensive and a maintenance-free means of solar water heating. These heaters have been in use for a relatively longer time compared to the modern day, more sophisticated counterparts because of design simplicity and lower cost. The earliest evidence of their deployment dates back to the late 19th century, when they were being used in farms and ranches in Texas, USA [1]. Smyth et al. [1] have given comprehensive detail on the chronological development of ICS collector type heaters. Better aesthetical value, easy integration in roof structures and good performance in diffuse radiation are added features that have pegged the ICS collector to endure the test of time. The ICS is one of the types of flat plate collector in which the storage tank is directly attached to the absorber plate instead of serpentine tubes or risers (see Fig. 1a).

The integrated collector storage solar water heater (ICSSWH) is the prime application of the study of natural convection in an inclined cavity. A considerable amount of research spanning over five decade on the topic has made it one of the classic heat transfer case studies, similar to flow across a cylinder and aerofoil in fluid mechanics. The built-in storage heater can also be viewed as an assembly of two natural convection cavities. In the heater under consideration, the air cavity (space between absorber plate and glass cover) sits on top of a water cavity (storage tank). From a convection standpoint, at any given angle of inclination of the heater, the behavior of both the cavities is nearly opposite. The reason is the difference in the magnitude of operating Rayleigh numbers, and the likeliness of having dissimilar geometrical dimensions (aspect ratios). The contrast is further enhanced owing to the fact that the water storage tank gets heated from the top surface, while the opposite is true for the air cavity. These differences coincidentally favor the pattern of required heat transfer. To be more specific, a lower Nusselt number on the air cavity side is desirable, as it weighs the heat lost to ambient. On the other hand, a higher Nusselt number favors the water cavity, as it quantifies the heat gain by water. The desired opposite performances, by chance, exactly go hand-in-hand with the actual behavior.

The cumulative efficiency of the ICS heater is merely the fraction of heat gained by the water tank over the total amount of energy incident upon it. Losses from the sides and the

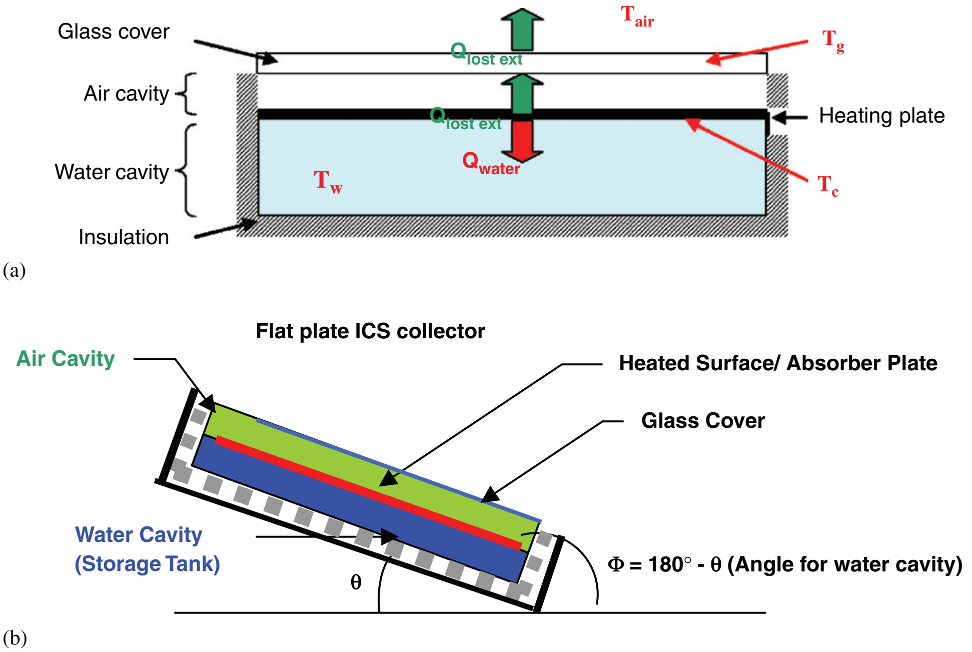

Fig. 1. (a) Schematic diagram of ICSSWH and (b) θ is the angle of inclination of heater, Φ is the angle for natural convection study, $\Phi = \theta$ for air cavity, $\Phi = 180^\circ - \theta$ for water cavity.

top (glass side) impede the useful heat gain and thus account for the decline in efficiency. Losses from the insulated sides of the heater are insignificant as they make about 5% of the total, as reported by Duffie and Beckman [2]. Edge losses for heaters with higher surface frontal areas are near negligible compared to vessels of greater thicknesses. It is, therefore, the dominating 95% losses from the top (air cavity side) that draw attention. Flat plate collectors for domestic application generally have heat loss coefficients of 5.5 $W/m^2 K$ for best selective surfaces to 10–11 $W/m^2 K$ for plain black absorber surfaces [3]. Emissivity, thus, is a crucial factor in determining the total heat loss value. In the present research, for the sake of simplicity, only convective losses have been considered.

Previous investigations on natural convection in inclined cavities demonstrate variation of the heat transfer coefficient (HTC) with the angle of inclination. Bearing in mind that a flat plate collector can have a variable angle of orientation, based on the geographical latitude of its location, the reason for the present investigation is vindicated.

Duffie and Beckhman [2] suggest the optimal angle to be 0.9 times of the latitude of the location. The maximum latitude for flat plat heater application would be 70° (Norway, Canada, etc.). The inclination of the heater can be as much as latitude $\pm 20^\circ$ to favor winter or summer collection [4]. This asserts the collector tilt can take values from 0° in equatorial regions to 90°, in regions of extreme latitudes. The present study will cover the behavior of both cavities (air and water) at collector angles from 0° to 90°.

In previous studies of inclined cavities, the angular variation of 0–180° has been investigated. This range, providentially, has aided the current investigation, which also encompasses the same angular sweep. Common convention for the angular position of an

inclined cavity is 0° when heated from below and 180° for heating from the top. For all practical inclinations of the water heater, the air cavity will operate in a range of 0–90° while the water cavity will have a range of 90–180°. Fig. 1b elucidates the angles for the air and the water cavity.

Unlike the angle of inclination, which is not a design parameter but is instead a design constraint locked to the geographical latitude, the aspect ratio can be tuned to achieve optimum performance of both air cavity and water tank. The angle of inclination of the heater and the aspect ratio are interdependent parameters. Therefore, for an optimal design, at different angle of inclinations, different aspect ratios are anticipated. The output temperature requirement and the rate of water consumption are also critical design parameters as they govern the thickness of the water storage tank. For this pilot study, the thickness of the built-in storage collector developed for laboratory testing of was determined in light of previous studies by Muneer and co-workers [5–9] and considering Edinburgh conditions.

Efforts to apply the knowledge of inclined cavity research on the design of flat plate collectors have been few. Buchberg et al. [4] were the first to link the outcome of research for minimizing the air cavity losses. The optimization studies for flat plate heater design have so far considered the imposed solar irradiance, temperature requirement and storage capacity as the main governing parameters. The effect of the angle of inclination on the performance of the heater so far has been neglected (to the author's knowledge). The present study aims toward optimization of the heater primarily from the knowledge of the angular performance as thus can be used to evaluate the performance of water heaters in various locations.

2. Natural convection in inclined cavities: a review

Over five decades of study has provided a deep insight to inclined cavity behavior, rendering it a well documented and widely explored area of research. The dependence of several influential parameters, however, compounds the uncertainty in prediction of heat transfer. A dimensionless analysis shows that the average Nusselt number depends upon the Rayleigh number, Prandtl number, vertical and horizontal aspect ratios, angle of inclination Φ and the end wall boundary conditions. In the case of solar heaters, air is the working fluid for the heat losses from top for which the Prandtl number is nearly constant (0.71). This simplifies the analysis to some extent. Studies on vertical air layers and horizontal slots have been studied far more than inclined cavities.

The principal investigation on inclined cavities was carried out by De Graaf and Van der Held [10] in 1953. Dropkin and Somerscales [11] followed the research and conducted numerous experiments involving liquids, the Rayleigh number range for which was 10^5–10^9. Increasing popularity of solar heaters in the early 70's encouraged Hart [12] to explore stability of the flow in inclined cavities, he did not, however, quantify the heat transfer. In the late 70's and early 80's, experimental research was performed by a number of researchers for determination of critical Rayleigh number and critical angle for cavities with high aspect ratios (H/L) [13–18]. The following decade saw a boost in progress, owing to the increase of computing power. Initially, only low Rayleigh number and small aspect ratios were investigated. More complicated studies, involving higher *Ra* numbers and aspect ratios, were picked up as passage of time gave way to more robust computing machines. In the 80's, the knowledge of flows was extended by numerical investigation of

three-dimensional (3D) aspects [19–22]. The influence of variable fluid properties and radiation was later inspected by Zhong et al. [18]. Recently, the study of cavities has been broadened by additional variations that include electromagnetic effects [23], variations of geometry such as effect of curved wall [24], addition of partitions, shallow or long cavities with aspect ratio less than 1 [25] and changes in the boundary conditions such as spatially varying temperatures [26]. The wide-ranging work of Ozoe et al. [19–22] is a proven cornerstone of the subject. His work includes theoretical (2D, 3D), experimental and photographic proof of the long rolls generated.

Even for a simple inclined cavity exclusive of variations, the intricate nature of flow itself has lead to the segregated regimes of studies. Each area, classified by certain Rayleigh number and aspect ratio range, was chosen by different researchers. Therefore, a study to assess and quantify the results of all the regimes, to establish a collective and comprehensive inclined cavity behavior has not been complied to date. To get an insight into the nature of inclined cavity and its response to different angles and aspect ratios, an attempt has been made in this paper to summarize the related earlier work.

To date heat transfer has been examined experimentally up to $Ra = 10^8$ [27]. Areas related to turbulent behavior for high aspect ratios of cavities still remain vague and unexplored. Higher values of both, the aspect ratios and Ra number lead to instabilities, the numerical solution of which also becomes complicated, if not impossible. Different thermal boundary conditions have been employed in the study of cavities. Two extreme limits known for the boundary conditions are perfectly insulation or zero heat flux (ZHF) and perfectly conducting or linear temperature profile (LTP) [28]. The present study only deals with ZHF.

For a vertical cavity, the flow has been categorized in three distinct regimes, namely conductive, transition and boundary layer regimes. Although these regimes can be identified in inclined cavities as well, they are more clearly defined and researched for vertical and horizontal orientations. These regimes depend upon the strength of the Rayleigh number. When the Rayleigh number is less than the critical value, conduction is the dominant if not the only mode of heat transfer. Beyond this value, the flow enters a post-conductive or transient regime. In this regime, advection takes over conduction as the dominant mode and a circulation pattern engulfs all of the fluid inside the cavity. At very high Rayleigh numbers, the cellular flow is further intensified and becomes concentrated in thin boundary layers adjoining the sidewalls. Termed as the boundary layer regime, at this stage the core becomes stagnant although additional cells can develop in the corners and the sidewall boundary layers.

For a 3D study of the inclined cavity, two aspect ratios have been defined (see Fig. 2). The vertical aspect ratio is the height to length ratio ($A = H/L$) and has been the focal geometrical parameter for nearly all previous studies. The other aspect ratio is the cavity width to the cavity length ($A_{\mathrm{H}} = W/L$) ratio, more commonly referred as the horizontal aspect ratio [13]. As long as the horizontal ratio is large, the dependence of flow on this parameter is negligible and is thus ignored in this text. The term 'aspect ratio' (A) unless defined, hereafter would imply a vertical aspect ratio. Flat plate collectors generally have an aspect ratio ($A = H/L$) above 12 for the air cavity. Emphasis, therefore, is focused on studies close to these ratios which are classified as medium and large ratios.

The previous work done on cavities is summarized and has been split into two sections. The first section examines the cavity behavior in the range of angles 0–90° (see Table 1), while the subsequent section epitomizes behavior in the range 90–180°. A comprehensive review on inclined cavities can also be referenced from the review report of Yang [37].

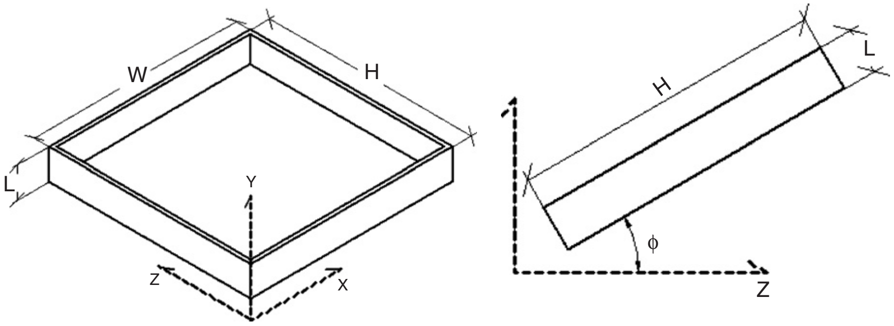

Fig. 2. Cavity is shown in 3D with the coordinate axis. The inclination angle remains in the Y–Z plane.

The objective in the study of cavity is the evaluation of the Nusselt number, which is directly related to the strength of the Rayleigh number and aspect ratio. For inclined cavities, it has been reported to be a function of both Ra and Φ independently rather than $Ra\cos\Phi$. Clever [38], however, demonstrated analytically that, provided two conditions are satisfied, the Nusselt number is a function of $Ra\cos\Phi$ only. The first condition is that the Prandtl number is infinite; the second condition is that fluid flow and temperature fields are independent of the distance along the cavity height. Hollands et al. have shown that the first condition can be relaxed. The regression by Hollands, which considers the Nusselt number to be a function of $Ra\cos\Phi$, shows excellent agreement to experimental data.

2.1. *Cavity behavior in range $\Phi = 0$–90°*

The flow behavior between 0° and 90° is fairly complicated and, therefore, has been subjected to extensive research. In this range, two types of flow instabilities exist, one is the static top heavy instability associated with the horizontal case when the angle is near 0° and second is the gravitational buoyancy associated with the vertical case. The cavity is termed as horizontal when $\Phi = 0^\circ$ and vertical when $\Phi = 90^\circ$. At vertical orientation, the direction of the temperature gradient is perpendicular to the gravity force and any finite Rayleigh number would cause the circulation motion of the flow in the cavity. However, for small Rayleigh numbers, $Ra \leqslant 1000$, the buoyancy driven flow is weak and heat transfer is primarily by conduction, thus implying the Nusselt number value again is unity [39].

For horizontal cavities (heated from below), the Rayleigh number has to reach a certain value before advection begins. This value is also termed as the critical Rayleigh number, which is reported by Hollands and co-workers [29,30] as $Ra_c = 1708$ for H/L, $W/L \gg 1$. Another value for horizontal cavities, $Ra_c = 1080$, has also been suggested [40]. For lower values than critical, heat transfer takes place through diffusion (conduction) only as viscous forces overcome any advection. When the Rayleigh number exceeds the critical value, the flow becomes unstable and series of convective 3D rolls are formed. These rolls are more commonly known as Benard cells. In case of inclined cavities, the multicellular convection arises when the Rayleigh number exceeds $1708/\cos\Phi$. Ozoe et al. [19–22] has photographically shown, using aluminum powder as a tracer that each of these rolls is confined to a rectangular volume whose dimensions do not change with inclination, i.e., each fluid particle remains within the cell. These cells not only appear along the length but also the width of the cavity. The width of the cell is experimentally shown by Dubois and

Table 1
Details of previous work on inclined cavities

Researcher/s	Aspect ratio range	Ra range	Results
De Graaf and Van der Held [10]		10^3–10^5	Longitudinal rolls were observed. The roll retained till $\Phi < 20$ and persisted Rayleigh number of 30,000
Dropkin and Somerscales [11]		10^5–10^9	Prandtl number has significant effect on the heat transport Aspect ratio has no effect on the Nusselt number
Hart [12]	$A > 25$	$Ra \approx 5000$	Longitudinal rolls with axis directed up slope. As "Pr" or "A" is lowered, Φ_{CR} reduces
Hollands and co-workers [29,30]	44 and 48	Close to but above $Ra_c = 1708$	At critical angle, heat transfer changes from one mode to other mode. Heat transfer rate decreases steadily with increasing angle of inclination up to 90°
Catton et al. [31]	1 and above	$Ra = 10^6$	Using a Galerkin method, it was found that the numerical solution to inclined cavities becomes unstable at angles $<30°$
Elsherbiny and co-workers [13,14,28]	5–110	$10^2-2\times10^7$	Developed heat transfer correlation for angle 60° and suggested linear interpolation between 60° and 90°
Ozoe et al. [19–22]	1–15.5	3×10^3–10^5	Angle of inclination at critical conditions is a strong function of the aspect ratio and weak function of the Ra number
Arnold et al. [32]	1, 3, 6 and 12	Up to 10^6	Minimum heat transfer between horizontal and vertical orientations is associated with the transition of the flow motions Transition between two motions does not superimpose Transition between the two motions changes for differing aspect ratios
Schinkel and Hoogendorn [33]	6–27	Up to 4×10^6	Nu number increases steadily with the decreasing angle of inclination
Linthrost et al. [16]	0.25–7	5×10^3–2.5×10^5	Transition from stationary two-dimensional to three-dimensional flow occurs with increasing angles of inclination for aspect ration larger than 1
Chen and Talaie [34]	1–10	10^3–10^7	Decreasing the angle of inclination from 90 to 0 the Nu number increases first but then decreases after reaching a peak value The peak of Nu number depends upon Grashof number
Hamady et al. [15]	$A = 1$ $^*A_z = 10$	10^4–10^6	Reducing the angle below 70° reduces heat transfer coefficient until a local minimum value is reached between 30° and 20°. Heat transfer then increases again till it reaches a weak maximum at zero
Kuyper et al. [27]	1	10^4–10^{10}	The Nusselt number shows a strong dependence on the orientation of the cavity and power law dependence on the Rayleigh number
Soong et al. [35,36]	4, 3 and 1	1×10^3–2×10^4	As the Ra number increases the transition angle also increases for a fixed aspect ratio Imperfect wall boundary conditions give better estimate with experiments
Yang [37]	40, 20 and 15.5	$4\times10^3-9\times10^3$	Imperfect boundary conditions (non-isothermal walls, transient BCs) are not a fix to inappropriate results 3D CFD analysis gives true results for higher aspect ratios

Berge [41] to remain equal to cell height for a Rayleigh number up to 10 times the critical value in the case of large-Prandtl number fluids [22]. Oertel [42] carried out experiments for nitrogen ($Pr = 0.7$) and found that the number of roll cells in a $4 \times 10 \times 1$ horizontal box changed from 10 to 9 at $Ra = 2300$, to 8 at 5680 and to 7 at 8900. On the other hand, for silicone oil ($Pr = 1780$), the number remained at 10 up to $Ra = 12{,}000$. Each cell rotates with a sense of rotation counter to its adjacent cell. As the angle of inclination is increased the strength of rolls with axis parallel to x-axis increases. Cells with axes parallel to the height—axis (up slope axis) tend to get weak and finally break up with increasing inclination. Ozoe et al. have given a detailed account on the nature of the flow along with the finite difference solution of cell. The streak lines resulting from finite difference calculation for reduced domain give a noteworthy picture of the 3D nature of the flow (see Fig. 3).

It was also found that the minimum heat transfer is associated with the angle where the flow changes its characteristic from multiple cells to a single cell. This angle is called the critical angle. The critical angle is dependent on both the Rayleigh number and the aspect ratio. It has been confirmed, however, that the aspect ratio has far more influence on the critical angle as compared to the Rayleigh number. Increasing aspect ratio shifts the critical angle toward the vertical orientation 90°. In a paper by Soong et al. [35], it has been validated that the transition point of the flow also moves to a higher angle as the Rayleigh number increased.

Table 2 lists the values of critical angle at various aspect ratios. As the angle is increased from horizontal to vertical it is found that the flow nature is 3D before the critical angle is reached, reliance on CFD results from 2D analysis, therefore, is inappropriate. Yang [37] has given comprehensive detail on the 2D CFD analysis compared with the results of experimental testing. After crossing the critical angle, the flow converts itself into single circulation roll with an axis parallel to the depth (in-page) axis. The flow rising along the hot wall joins the flow descending down the cold wall and vice versa to make a complete loop along the walls. The nature of this flow is 2D which can be tackled using 2D CFD analysis. Turning to Table 2, it can be noticed that for an aspect ratio >12 the critical angle is 70°, which implies that only the angular span of 20° between 70° and 90° can be analyzed using 2D CFD analysis. As most solar collectors would have an aspect ratio above 12, 3D CFD studies are essential for comprehensive analysis.

For medium to large aspect ratios cavities with vertical orientation, the effect of high aspect ratio is the delay in the departure of Nusselt number from unity to larger values of Ra. Hollands et al. have also reported that for increasing aspect ratio, the contribution of convective heat transfer to the average Nusselt number becomes vanishingly small so that the average Nusselt number reaches unity.

Summarizing all the results, the established trend in a cavity with high aspect ratios would be the steady decrease in the Nusselt number with increasing angle till a local minimum is reached. This point marks the critical angle. The Nusselt number from this point onward escalates, but with a gentle slope. This general trend for high aspect ratios is depicted in Fig. 9.

2.2. *Cavity behavior in range $\Phi = 90$–$180°$*

To date the work done on cavities for $90° \leqslant \Phi \leqslant 180°$ has witnessed lesser attention as compared to the previous range. The cavity at 180° indicates "inverted horizontal cavity",

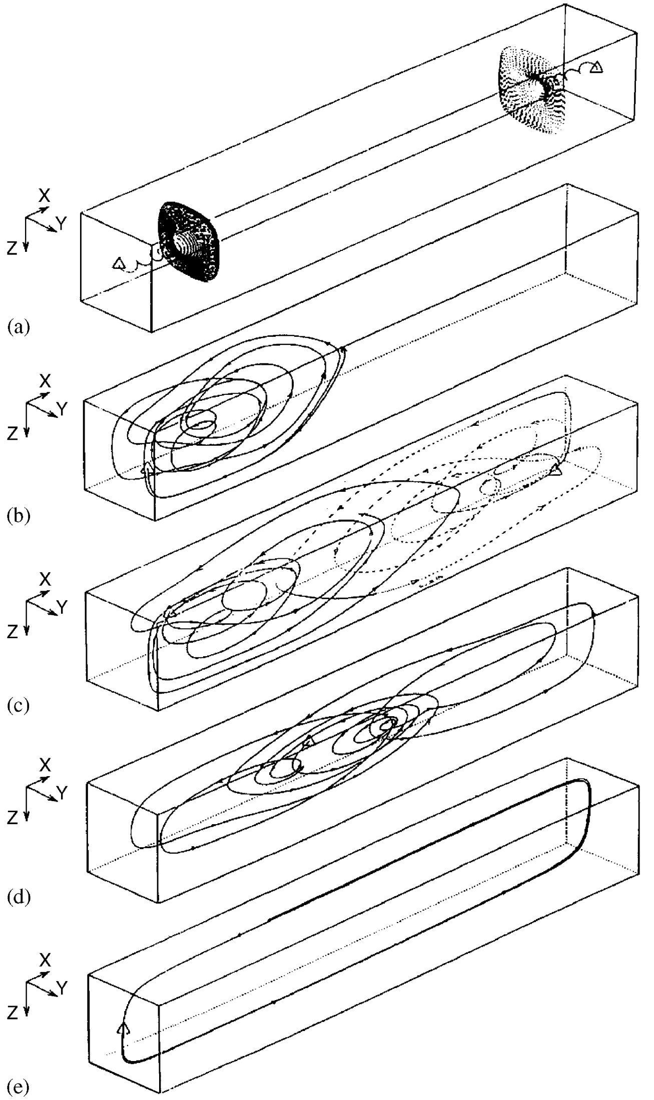

Fig. 3. Perspective view of streak line from 3D finite difference calculation of Ozoe et al. with free–free cell boundary condition. The angle of inclination lies in the X–Z plane: (a) $\Phi = 0^{\circ}$, (b) $\Phi = 20^{\circ}$, (c) $\Phi = 30^{\circ}$, (d) $\Phi = 40^{\circ}$ and (e) $\Phi = 90^{\circ}$. The original figure reproduced from Ozoe et al. [22].

Table 2
Critical angle for various aspect ratios [40]

H/L	1	3	6	12	>12
Φ_{CR}	25°	53°	60°	67°	70°

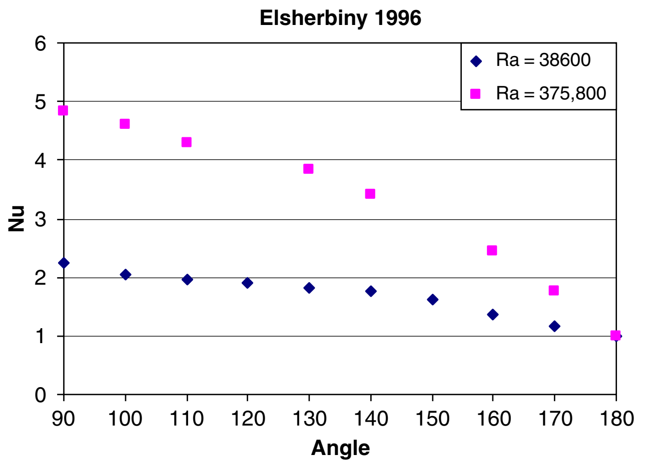

Fig. 4. Experimental results for cavity ($A = 20$) by Elsherbiny [28] for two different values of Ra.

i.e., being heated from the top. In terms of convection strength, this position is indicative of the worst-case scenario. The Nusselt number for a cavity at $\Phi = 180^\circ$ is "1" according to study by Hamady et al. [15]. This value implies pure diffusive heat transfer. The Nusselt number remains unity at this angle, irrespective of the strength of the Rayleigh number for ZHF boundary conditions. For LTP boundary conditions, however, the Nusselt values depart from unity for $Ra \approx 10^5$, as suggested by Elsherbiny [28] in his experimental study of $A = 20$ and 80. Advection begins with the slightest of rotation of the cavity toward the vertical position. Previous studies have shown velocity along the walls to increase as the cavity is rotated from "inverted horizontal" (180°) to a vertical position (90°). This increase in velocity accounts for the increase in Nusselt number. Studies by Ozoe and Elsherbiny have shown this increase being sinusoidal. The rate of increase of the Nusselt number with the Rayleigh number also depends upon the angle of inclination. The higher the angle the lower is the slope. This trend is shown in Figs. 5 and 6.

In general for the range of the $\Phi = 180-90^\circ$, the behavior has marginal intricacy as compared to its mirror range. The nature of the flow is a 2D hydrodynamic circulation with axis of rotation parallel to the depth of the cavity (x-axis). This flow pattern carries on until the critical angle, after which it switches over to Benard cells.

It is also a feature of flow in this range that for any given value of Rayleigh number, the departure of Nusselt number from unity is delayed with the increase in the angle (90–180°). For any given angle and Rayleigh number, the Nusselt number decreases with the increase in the aspect ratio. The results of Elsherbiny are depicted in Figs. 4–6 and sum up the activity in this range. The increase in the delay in departure of the Nusselt number from unity with increasing angle can be noticed in Figs. 5 and 6. The effect of the increasing aspect ratio is the reduction of Nusselt number for the same operating conditions (Rayleigh number and angle of inclination) [28]. As Φ is increased the change to turbulent flows occurs at higher values of Rayleigh number.

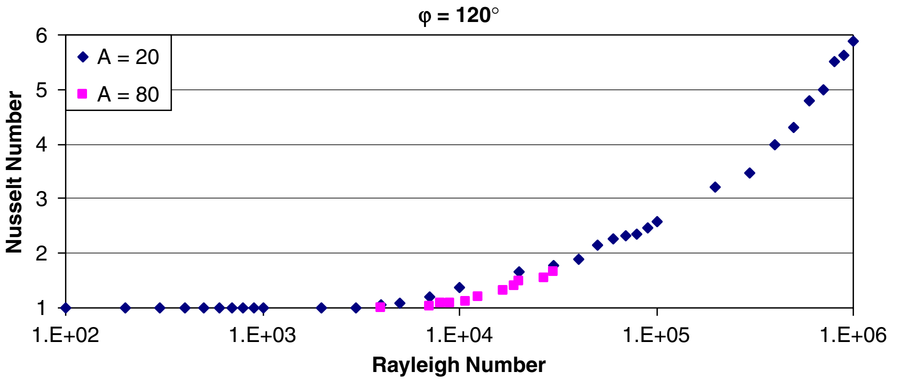

Fig. 5. Experimental results for $A = 20$ and 80 by Elsherbiny [28] for different values of Ra at $\Phi = 120^{\circ}$.

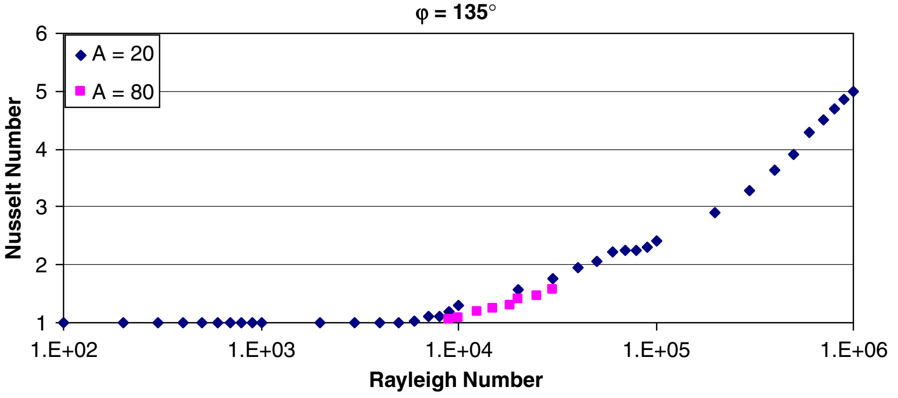

Fig. 6. Experimental results for $A = 20$ and 80 by Elsherbiny [28] for different values of Ra at $\Phi = 135^{\circ}$.

2.3. Air cavity behavior for the tested water heater ($0^{\circ} \leqslant \Phi \leqslant 90^{\circ}$)

Having examined the nature of the flow for cavity at all angles, focus is turned toward the air cavity in the solar water heater which for all locations would practically operate within an angular range of 0–90°. The Rayleigh number inside the air cavity is a transient parameter and varies in the range $Ra = 0$ (at the start of the charge) to $Ra = 10^5$[1] (at peak temperature value of absorber plate). The strength of the Rayleigh number depends upon the charging time or more precisely the temperature of the absorber and the cover plate. For each geographical location, a yearly mean Rayleigh number value of operation can be allotted based on the meteorological data. This means Rayleigh number value will depend upon the ambient weather conditions, including cloud cover, the incident radiation, wind speed and ambient temperature. For the purpose of lab testing, an ICS heater was developed the details of which are described in a later section. The air cavity for the

[1]The mentioned peak value of Rayleigh number was recorded from the experimental tests conducted in the laboratory.

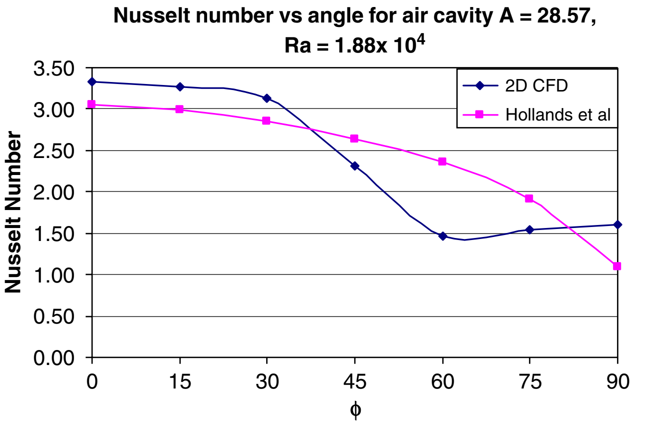

Fig. 7. CFD results from 2D analysis showing the behavior of Nusselt number with the tilt. The results from regression by Hollands have also been plotted.

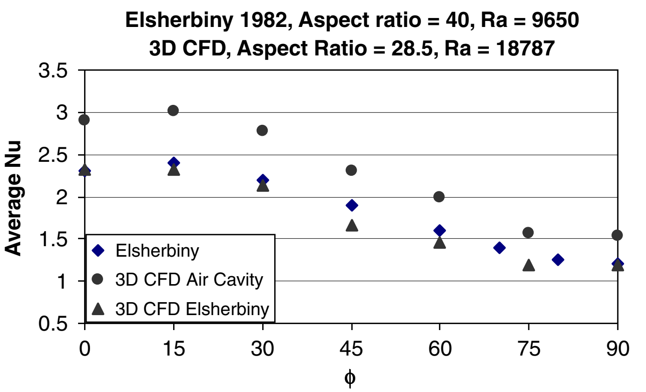

Fig. 8. Results from the study of Elsherbiny, 1982, showing a steady decline in the Nusselt number.

developed heater had the dimensions $1\,\text{m} \times 1\,\text{m} \times 0.035\,\text{m}$, fixing the horizontal and vertical aspect ratio to a value of $A = 28.5$. CFD analyses for the air cavity was carried out for a chosen value of Rayleigh number $Ra = 1.88 \times 10^4$ for all angles between 0° and 90° with 15° intervals. The value of Rayleigh number represented an absorber plate temperature of $35\,^\circ\text{C}$ and a cover plate temperature of $30\,^\circ\text{C}$.

In light of the previous studies, a steady decrease in the Nusselt number with the increase angle Φ can be anticipated. To save computational effort, 2D CFD analysis was carried out initially. The results from the analyses are plotted and compared to results from the correlation by Hollands et al. in Fig. 7.

The established results of Elsherbiny [13,14] for the closest aspect ratio to the present study are plotted below for comparison with the CFD results.

The results in Fig. 7 indicate 2D CFD results deviating from the true behavior when compared to the experimental results of Elsherbiny shown in Fig. 8. A separate 2D analysis was carried out in addition for the air cavity with an aspect ratio of 20. The sudden dip,

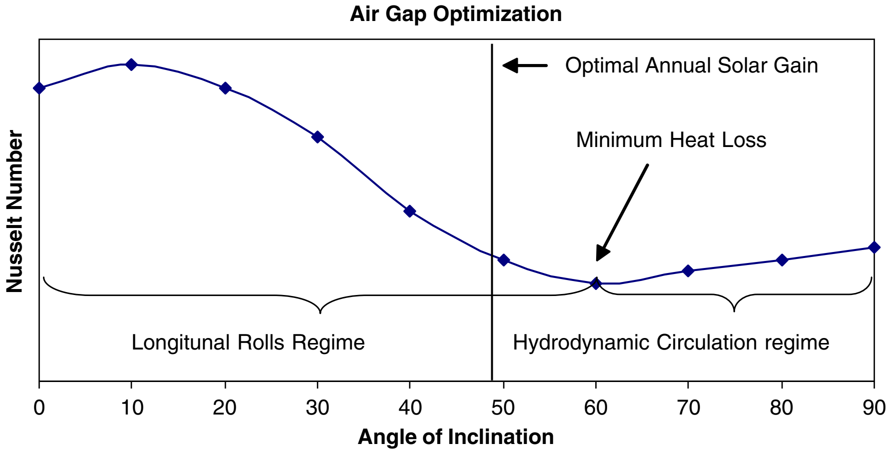

Fig. 9. The generic Nusselt number trend for higher aspect ratios cavities.

instead of a gradual decrement in the Nusselt number curve was again observed. This sudden dip is a characteristic feature of results from 2D CFD analysis and has been also reported by Yang [37]. Even though the upper and lower limits of the Nusselt number correspond to the regression values, 2D CFD in general fails to predict the gradual decline in the Nusselt number and thus furnishes an incorrect value of the critical angle. 3D analysis is, therefore, the only solution in this range. This does not, however, imply that 2D CFD is utterly ineffective. It has been applied with success in the past but only in the domain of lower values of both aspect ratios and Rayleigh number.

To benchmark 3D CFD analysis, experimental results of Elsherbiny for an aspect ratio of $A = 40$ and $Ra = 9650$ were used. These were the closest available results in the reviewed literature that concurred with the dimensions of developed air cavity. Excellent conformance between the two was found (mean bias difference, MBD = 0.083 and root mean square difference, RMSD = 0.0136), thus confirming the mesh size to be reasonable and the choice of discretization schemes to be appropriate. A gradual decrease in the Nusselt number was observed till "Φ" reached the critical value, after which a slight increment was observed. Confidence can be taken in the result of 3D CFD analysis of the air cavity which showed a similar trend to the bench mark case. Fig. 8 depicts the 3D CFD results for both cases along side the experimental results of Elsherbiny. Higher values of Nusselt number in case of the air cavity were the consequence of a different aspect ratio and a higher Rayleigh number of operation. The outcome of the exercise is the critical angle, which lies around the 75° mark as can be noticed from Fig. 8.

Optimal design of an air cavity in the ICSSWH would require constraining of the Nusselt number to a lowest possible value. For the sake of explanation, in Fig. 9, a hypothetical description of the general trend of Nusselt number in high aspect ratio cavities is depicted. It shows that an ideal condition is achieved when the angle of inclination of air cavity would match the critical angle for that cavity. Keeping the critical angle of the air cavity as close as possible to the angle of inclination of the heater is, therefore, the objective. The design rule for the air cavity for ideal conditions would be $\Phi/\Phi_c \geqslant 1$. A value greater than 1 implies flow in the air cavity will lie in the hydrodynamic regime. Owing to the fact that multicellular regime augments heat loss more than the

hydrodynamic circulation regime; it is relatively a better option to have the angle of inclination fall in the later regime, i.e., after the critical angle. Considering Edinburgh, for which the optimal solar irradiance gain angle is 49°, Table 2 suggests an aspect ratio of 3 for critical angle. This low value of aspect ratio is impractical. Roof mounted ICS collectors generally have surface areas of $1\,\text{m} \times 1\,\text{m}$. An aspect ratio of 3 would imply the cavity thickness of $L = 33.3\,\text{cm}$. This high value of cavity thickness has its own setback.

CFD analysis for the air cavity (Fig. 8) had revealed the critical angle around 75°. Decreasing the aspect ratio from the current value of 28.5–20 would decrease the critical angle to a value closer to the angle of inclination of 49°. Decreasing the aspect ratio means an increase in the cavity thickness "L", which corresponds to an increase in the Rayleigh number. A higher Rayleigh number on the other hand promotes higher heat loss by convection. Conduction resistance would, however, have to be taken into consideration to quantify these heat losses. To sum up, an increase in the cavity thickness to lower the critical angle would not be an efficient practice to minimize heat losses.

The optimal thickness is, therefore, the maximum thickness of the cavity for which the value of the Nusselt number would remain 1 or close to it. As mentioned previously $Ra_c = 1708/\cos\Phi$ is the maximum value of Rayleigh number for which $Nu = 1$. Assuming a temperature difference of 5 °C between the absorber and cover plate, crude value of cavity thickness from the critical Ra_c was evaluated and was found out to be $L \approx 1.74\,\text{cm}$. For higher values, Rayleigh number would increase suggesting convection overtaking conduction. Below this value the conduction resistance would become smaller implying higher heat loss through conduction.

Limiting the Rayleigh number of operation inside the cavity close to a critical value would improve performance. However, the difference of 5 °C between the plates is not a constant value and, therefore, a definite length cannot be suggested for the entire period of operation. The range of the Rayleigh number depends upon the absorber plate and the ambient temperatures. The absorber plate temperatures are in turn a function of imposed heat flux, heat loss through the air cavity sides, charging time and thickness of the tank. It would not be possible to have a constant optimum thickness of cavity for all times of operation of the heater to reduce the heat losses. With the increase in the Rayleigh number the minimum heat loss coefficient shifts toward lesser thicknesses. Temporal data will be required for the heater tested in real conditions for a large period of time to evaluate an average length that would improve the life-cycle performance of heater.

It has become customary to make the magnitude of "L" approximately 1–2.5 cm. Hottel [43] has suggested through his experiments that increasing the air space beyond 1.27 cm had little effect on reducing the conductance, while Buchberg et al. [4] have shown that the spacing between the tilted hot solar absorber and successive glass covers should be in the range 4–8 cm to assure minimum gap conductance.

The air gap optimization itself is a topic of in-depth research involving several parameters, chiefly the transience of the Rayleigh number. The highlight of the air cavity results is the decrease in the Nusselt number with the increase in Φ for aspect ratios of practical interest.

3. Water storage tank behavior for the tested water heater ($90^\circ \leqslant \Phi \leqslant 180^\circ$)

The water cavity in an ICS collector operates within the angular range 90–180°. The aspect ratio of the water tank for the tested ICS heater in the laboratory was $A = 20$.

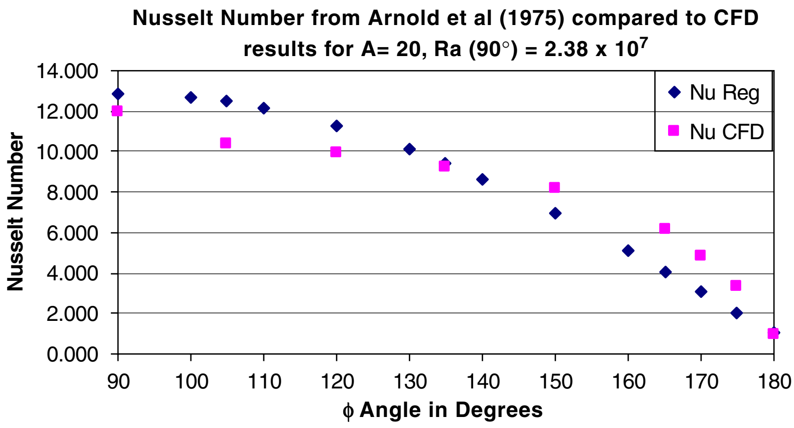

Fig. 10. CFD results show good agreement compared to the regression by Arnold.

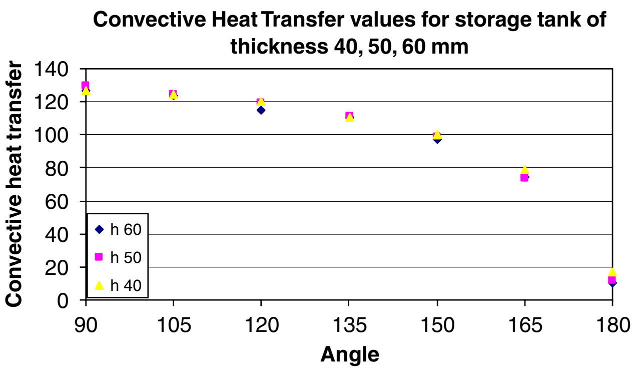

Fig. 11. CFD results show similar convective heat transfer coefficient value for all the thicknesses analyzed.

During the experimental tests the Rayleigh number range was found to be with in 4.5×10^5–3.3×10^7. This range was evaluated on the basis of a recorded peak 7 °C temperature difference within the water storage. CFD analysis was carried out for the water cavity for $Ra = 2.38 \times 10^7$. Results at angular increments of 15° were recorded to cover the range 90–180°. These results were compared to regression by Arnold et al. The scaling law derived by Arnold et al. drawn in Fig. 10 is reasonably accurate with maximum deviation of less than 10% reported by Elsherbiny [28]. As discussed in the previous sections the nature of the flow in the angular domain of the water cavity is 2D; therefore, to save computational effort, 3D analysis was not performed.

In Fig. 10, CFD and the results from the correlation by Arnold et al. are compared. A high degree of conformance between the two (MBD = 0.213 and RMSD = 0.157) testifies the validity of 2D CFD results. The Nusselt number decreases monotonically as Φ is increased. The reason being the component of velocity along the isothermal walls of the cavity reduces with the increase in angle. The result is a reduction of the velocities which in effect causes decline in the Nusselt number value. Fig. 18 shows the velocity contours from the CFD results, the strength of the velocity can be seen decreasing with angle.

The important conclusion from this result is that the performance of the water tank is poor in terms of heat gain through convection when at inverted horizontal position ($\Phi = 180^\circ$). The performance gets better as vertical orientation is approached. Point of interest is that if the ICSSWH is inclined at 45°, i.e., the angle for the water cavity is $\Phi = 135^\circ$, the thermal efficiency of the heater is lower as compared to higher angle of inclinations ($\Phi < 135^\circ$). Increasing the angle further increases the efficiency.

CFD analyses for three different aspect ratios were carried out to get the best possible configuration for Edinburgh. Storage tank thicknesses of 40, 50 and 60 mm were analyzed. In order to compare the behavior of all three geometries, the convective HTC was plotted against the angle instead of the Nusselt number (Fig. 11).

The plot depicts that the difference in the thickness does not make a significant difference. In general, the 40 mm thickness water tank has a slightly higher value of convective HTC for most angles. The thickness of the heater, however, has greater influence on the overall thermal efficiency and the output water temperature. The temperature rise for the 40 mm tank would be higher as thermal mass is low. The characteristic of rise in temperature for all three tanks is explored in a later section.

4. Treatment of water tank as a cavity

The treatment of the water tank as an inclined natural convection cavity is a fairly generous assumption. Different boundary conditions on the water tank, i.e., isoflux on one side and quasi-adiabatic on the other three sides imply a different behavior. In the case of a conventional natural convection cavity, the driving factors for heat transfer are the two isothermal surfaces. Heat from the hot wall is transferred to the cold wall via convective current. The strength of convective current depends upon the Rayleigh number.

During charging of the heater, the water inside the tank acts as a thermal capacitor. The energy is absorbed and the water temperature rises with time, making it a transient process. A steady-state condition is reached when the losses equal the imposed heat flux. This occurs after the water temperature has reached a saturation value corresponding to the imposed heat flux. At this point, the resistance for the heat to flow into water from absorber plate exceeds the resistance to the air cavity side. The time for the system to reach steady state depends upon the depth of the cavity, insulation thickness and the angle. These differences suggest the implication of inclined cavity results to the water tank without manipulation would be invalid.

The assumption of the water storage tank as an inclined natural convection cavity was taken to gather the pilot results for the heat transfer inside the cavity. A transient CFD analysis for the water tank was carried out with the mentioned set of boundary conditions and similar results were obtained, i.e., the decrease in the Nusselt number with the increase in Φ. The details of the analysis have been excluded for the sake of brevity.

5. Optimal angle of inclination for Edinburgh

For evaluating the optimal angle and orientation for Edinburgh, 27-year irradiance data were processed. The graph depicts that maximum yearly solar irradiance gain is at an angle of 35° rather than 49° as predicted by the general rule of thumb [2]. The results indicate only a slight variation of total irradiance in the range of 30–55° (Fig. 12). The behavior of the ICSSWH in this range is of interest. From the study of cavities in the previous sections,

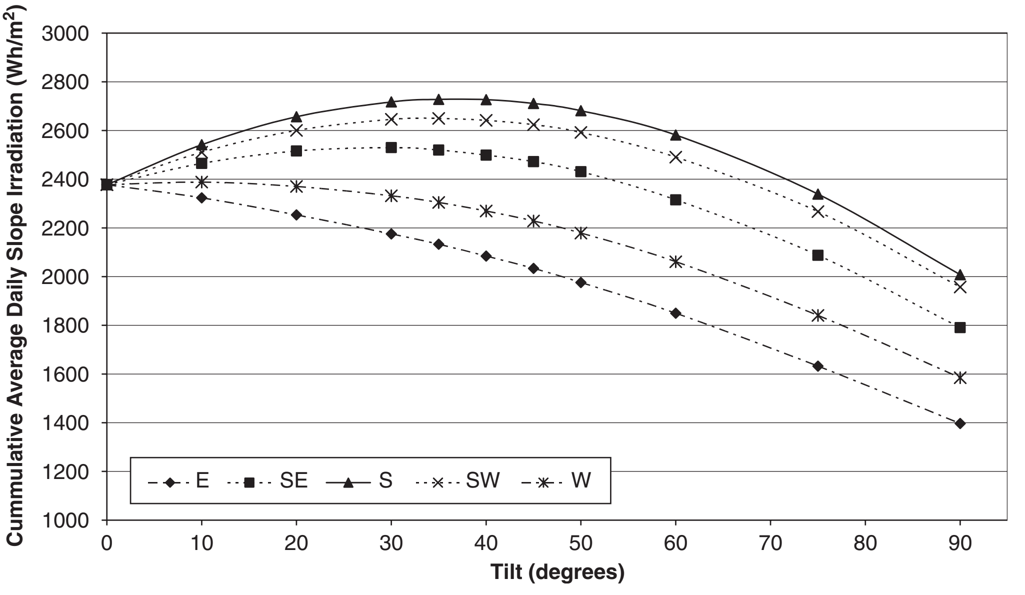

Fig. 12. The graph shows the slope irradiance with the tilt angle for Edinburgh, The plot was generated using 27-year data.

it can be inferred that the angle of inclination of 55° would thermally out-perform 35°. Higher Nusselt number for the water tank at $\Phi = 125°$ will promote heat gain. In addition, the lower Nusselt number for the air cavity at $\Phi = 55°$ would reduce the heat loss as compared to 30°.

Fig. 12 shows the average yearly output of solar irradiance for various directions and angles for Edinburgh. The slope irradiance for 35° and 50° facing south shows a difference of only 1.6% (irradiance values of 2727 and 2681 Wh/m^2, respectively). The Nusselt number value of water tank at 50° ($Nu = 9.48$), however, is greater than value for 35° ($Nu = 8.56$), a difference of 10.7%. This implies that the ICS water heaters inclined at 50° will perform better thermally compared to the heater mounted at 35°. The other advantages are that higher inclination would give the heater a seasonal bias during the winter months when the requirement of hot water is greater.

The collective efficiency of the heater at any angle of inclination would depend upon both the heat taken up by the water tank and the losses from the air cavity. In the previous section, both these components (air cavity and water tank) were studied independently and it was noted that the performance of both cavities is strongly dependent upon the angle of inclination.

The HTC for both cavities is shown in Fig. 13. The HTC for the air cavity is comparatively lower than for the water cavity, implying the air cavity having a small impact on the overall efficiency of the heater. The peak value of the convective heat loss occurs at the horizontal position ($\Phi = 0°$). In this situation, heat transfer to the water cavity is minimum while losses from the air cavity are maximum thus indicating a worst-case scenario. Best performance is witnessed when the water heater is at vertical orientation ($\Phi = 90°$). At this point, the losses through the air cavity are near minimum and the heat gained by the water is the highest.

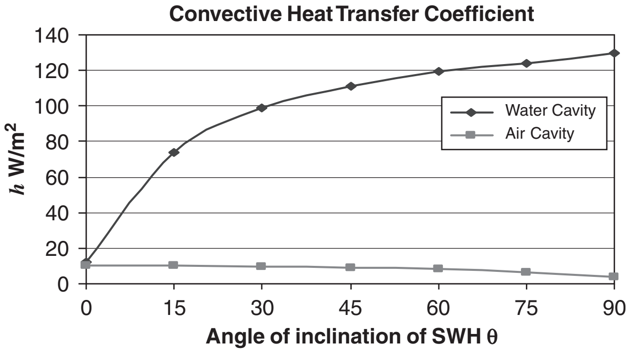

Fig. 13. Convective heat transfer value for both air and water cavity plotted with varying angle of inclination of the heater.

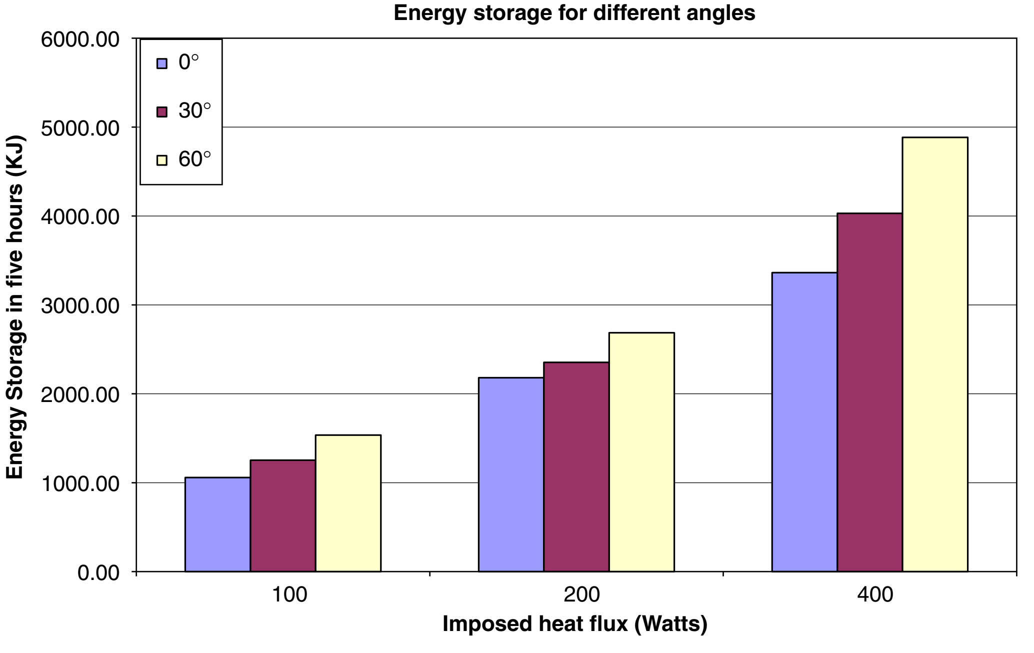

Fig. 14. The energy gain for angles 60°, 30° and 0° for different values of imposed heat flux.

Experimental results validate the claim for an increase in efficiency with the angle. The results are shown in Fig. 14.

The figure shows the accumulated efficiency of the heater for 100, 200 and 400 W for angles 0° and 30°. The performance improves with the increase of the angle. For regions of lower latitude, the ICSSWH would have a lower angle of inclination to achieve annual maximum solar gain. If the angle of inclination is increased by 5–10°, then the overall efficiency of the system would be increased despite trading off some radiation. Higher rate of draw-off from the heater would further improve the performance for an increased angle. Increasing the angle in higher latitudes although would also result in an increase in

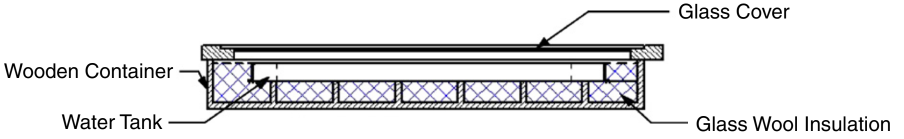

Fig. 15. Section view of the ICS collector developed in the laboratory.

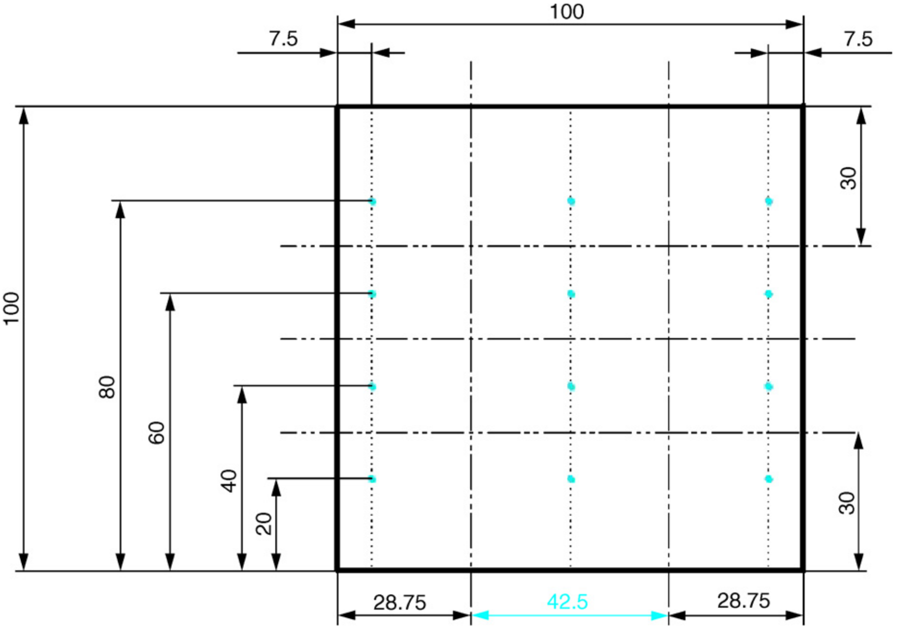

Fig. 16. Showing the location of the thermocouples (dots) inside the heater. The dashed lines indicate the boundaries of the control volumes used for average temperature calculations.

efficiency; this increase, however, would be marginal as compared to increase in lower latitudes.

6. Experimental investigation

A full-scale flat plate built-in storage collector was made for laboratory testing. The water tank was made out of stainless-steel sheet with a gauge thickness of 1.5 mm (see Figs. 15 and 17). Hardwood was used for the external casing, while glass wool insulation was used on the sides and the bottom on the water tank. Glass wool covering was 100 mm thick on each side. The gap between the absorber plate and the glass cover was 35 mm, which implies that air cavity has an aspect ratio of 28.5.

For the purpose of experimental testing, 12 K-type thermocouples were used to monitor the behavior of temperature rise inside the tank. The location of the thermocouples is shown in Fig. 16. A resistance heating rubber pad was placed on top of water storage tank for heating. Provision was made for a controlled power supply to have a measured amount of heat generated by the heating pad. For Edinburgh, although the peak value of solar

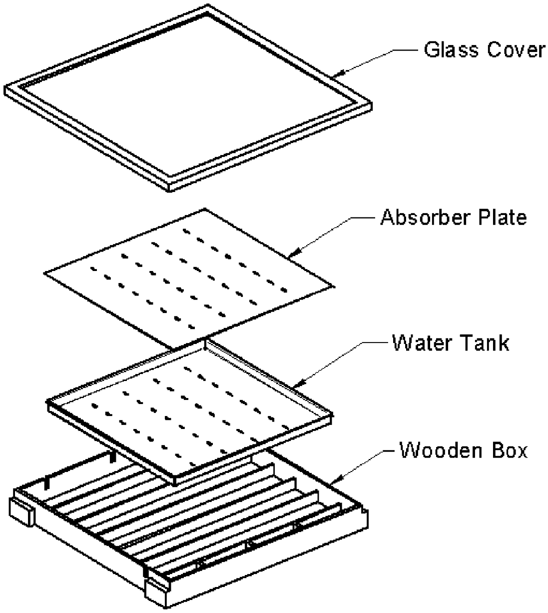

Fig. 17. Exploded view of the heater assembly.

irradiance is high and could reach well above 800 W on a bright sunny day, the majority of the heating season dwells around the 400 W mark. In view of these conditions, testing for heat fluxes was done for 100–400 W.

When the ICS heater is inclined, because of stratification, a variable temperature distribution develops inside the tank. In order to effectively evaluate an average temperature for the water tank, control volumes were assigned to each of the thermocouples in the region of their vicinity. A weighted average temperature was evaluated using a control volume approach. The dimensions of these control volumes are given in Fig. 16. Tests were carried out for heat fluxes of 100–400 W with an increasing interval of 50 W. The rise in the temperature was recorded after 10 min intervals. Each test was carried out until the system reached equilibrium, i.e., no further increase in the temperature was observed. All the heat input at this point was going into the losses. A thermal imaging camera (Therma-cam) was also setup to monitor the heat loss through of the glass cover surface. Alternating hotspots with relatively cooler regions in between were witnessed. Fig. 22 shows the Therma-cam images with the passage of time. The presence of hotspots can be attributed to presence of Bénard cells. A clearer picture of the cells would, however, require the use of sophisticated equipment and intricate photography techniques as discussed and conducted by Ozoe et al [21].

7. CFD analysis

The CFD analysis was done using Fluent 6.2 CFD software, while meshing was done using preprocessor Gambit 2.2. As the geometry was regular, quad structured mesh was easily employed. Quad mesh works well with quadratic upstream interpolation for convective kinetics (QUICK) scheme [44]. QUICK is a second-order discretization scheme

and gives fairly good results on a lower cell count when flow is aligned with the grid [44]. The mesh size is critical for CFD analysis especially when dealing with natural convection. Zhai and Chen [45] have given good detail on the effect of the error with the mesh size. For accuracy, the mesh size taken here is 1 mm. This was done to accommodate at least one cell within the boundary layer. As the Rayleigh number increases, the cellular flow intensifies and becomes concentrated in thin boundary layers adjoining the sidewalls. The gradients inside the boundary layer rise sharply, prompting the need for a finer mesh on the boundaries. The core region becomes thicker and is nearly stagnant. This is a major reason why researchers, having obtained good accuracy at low Rayleigh numbers, were not able to repeat the feat with same accuracy for higher values. At higher Rayleigh numbers as the boundary layer size is reduced the same mesh becomes relatively coarse.

CFD analysis of natural convective flow in an enclosed domain is intricate. The airflow is considered to be incompressible, and Boussinesq approximation is applied to simplify the flow governing equation. The Boussinesq approximation breaks the dependency of density on the local temperature by evaluating an equivalent change using a constant value for thermal expansion coefficient. All other thermophysical quantities were assumed to be constant. The thermal expansion coefficient can be treated as a constant in a small temperature range. This suggests that the Boussinesq approximation should not be used when the temperature differences in the domain are large.

The Rayleigh number for the study carried out for air cavity was $Ra = 1183$. For all, the CFD analysis carried out the flow has been considered laminar. The flow gets turbulent for a horizontal cavity at higher Raleigh numbers than 5×10^4 [46]. The boundaries for turbulent flows have been vividly defined for the case of a vertical cavity. There is no definite Ra number value which can be suggested for transition to turbulence flow as it depends upon the Rayleigh number, angle of inclination, and the aspect ratio. A ballpark figure for turbulence for an aspect ratio of 100 is $Ra = 3000$. While for aspect ratios of less than 10, it takes values of $Ra 2 \times 10^6$ [46]. The trend is that for higher aspect ratios, the flow gets turbulent even at lower Ra number values. For the air cavity, the assumption is valid as the transition to turbulence for an aspect ratio of 28.57 is in between $1 \times 10^5$and 2×10^5. For the water cavity, however, the transition to turbulence lies, for an aspect ratio of $A = 20$ and $Ra 3 \times 10^5$.

7.1. Governing equations

The general transport equation in integral form can be given as [45]

$$\frac{\partial}{\partial t}\int_V \rho\phi \,\mathrm{d}V + \oint_A \rho\phi V \,\mathrm{d}A = \int_A \Gamma \nabla\phi \,\mathrm{d}A + \oint_V S\phi \,\mathrm{d}V, \tag{1}$$

Unsteady + Convectic = Diffusion + Generation.

The above equation is the general transport equation and can be converted into flow and energy equations by replacing the variable φ:

continuity 1,
x-momentum u,
y-momentum v,
energy h_o.

7.2. Boussinesq approximation

In solving natural convection flows, faster convergence is achieved if the Boussinesq model is used. The Boussinesq model assumes density is constant in all solved equations, except for the buoyancy term in the momentum equation. The density may be represented by a linear function of temperature for small temperature differences and the change in density is related to the thermal expansivity, β, as [44]

$$\beta = -\frac{1}{\rho}\left(\frac{\partial p}{\partial T}\right)_p. \tag{2}$$

If β is approximated by

$$\beta \cong -\frac{1}{\rho}\left(\frac{\rho_\infty - \rho}{T_\infty - T}\right)_p, \tag{3}$$

then

$$\rho_\infty - \rho \cong \beta\rho(T - T_\infty). \tag{4}$$

In the above expression, density change is linked to the temperature change. This would make the momentum equation as

$$u\frac{\partial u}{\partial x} + v\frac{\partial u}{\partial y} = \beta\rho(T - T_\infty) + v\frac{\partial^2 u}{\partial y^2}. \tag{5}$$

Note that Boussinesq approximation can be used if it meets the following criteria:

$$\beta(T - T_{\mathrm{o}}) \ll 1. \tag{6}$$

7.3. Convergence criteria

In order to reach a stabilized solution, transient approach was used. Fluent Inc. recommends the following general criteria when solving natural convection flow in an inclined cavity:

$$\tau = \frac{L}{U} \approx \frac{L}{\alpha^2}(Pr\,Ra)^{-1/2} = \frac{L}{\sqrt{g\beta\Delta TL}}, \tag{7}$$

where L and U are velocity scales, respectively. A time step Δt is used such that

$$\Delta t = \frac{\tau}{4}. \tag{8}$$

The steady-state solution was first obtained with a low value of gravitational acceleration (0.981 or 0.0981) to drop down the value of the Rayleigh number to obtain a converged steady-state solution. Later this value was increased to the real value.

7.4. Mesh density

A structured hex mesh was used as the geometry of the heater was fairly regular 3D box. The advantage of quad mesh over the tetrahedral mesh is dual. Firstly, higher-order

discretization schemes such as QUICK can be applied and secondly a lesser number of cells are required to resolve to the same accuracy as would be required in case of tetrahedral elements [44]. This saves both computational effort and time. The mesh density for the 3D CFD analyses was kept $200 \times 200 \times 16$ for the aspect ratio of 28.5. For an aspect ratio of 40, it was kept to be $200 \times 200 \times 12$. Non-uniform mesh distribution was used which was not the case in previous studies. This helped resolve the boundary layer, where gradients were high and also kept the over all cell count low.

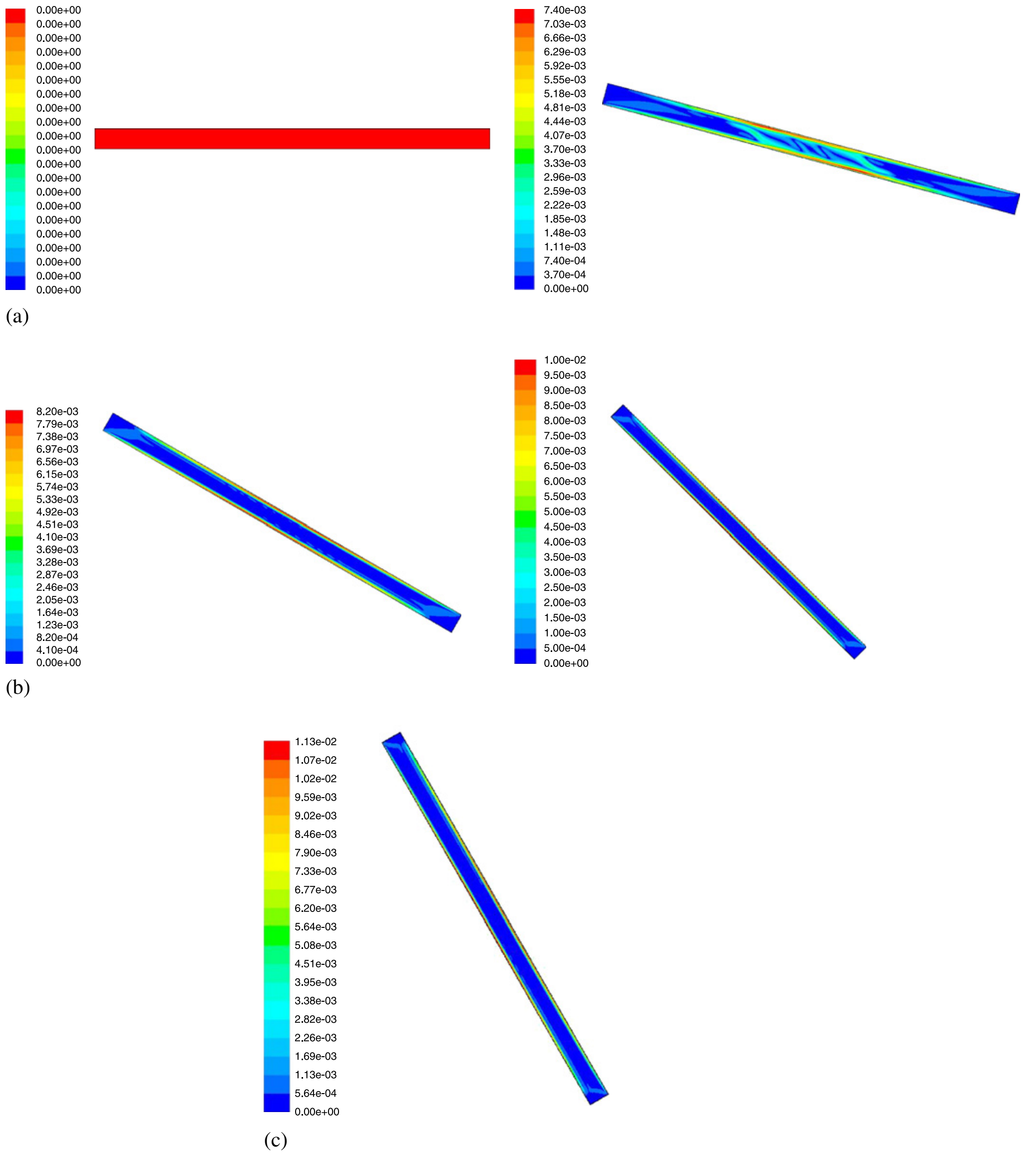

Fig. 18. Contours of velocity magnitude are shown for (a) 0° and 15°, (b) 30° and 45° and (c) 60°.

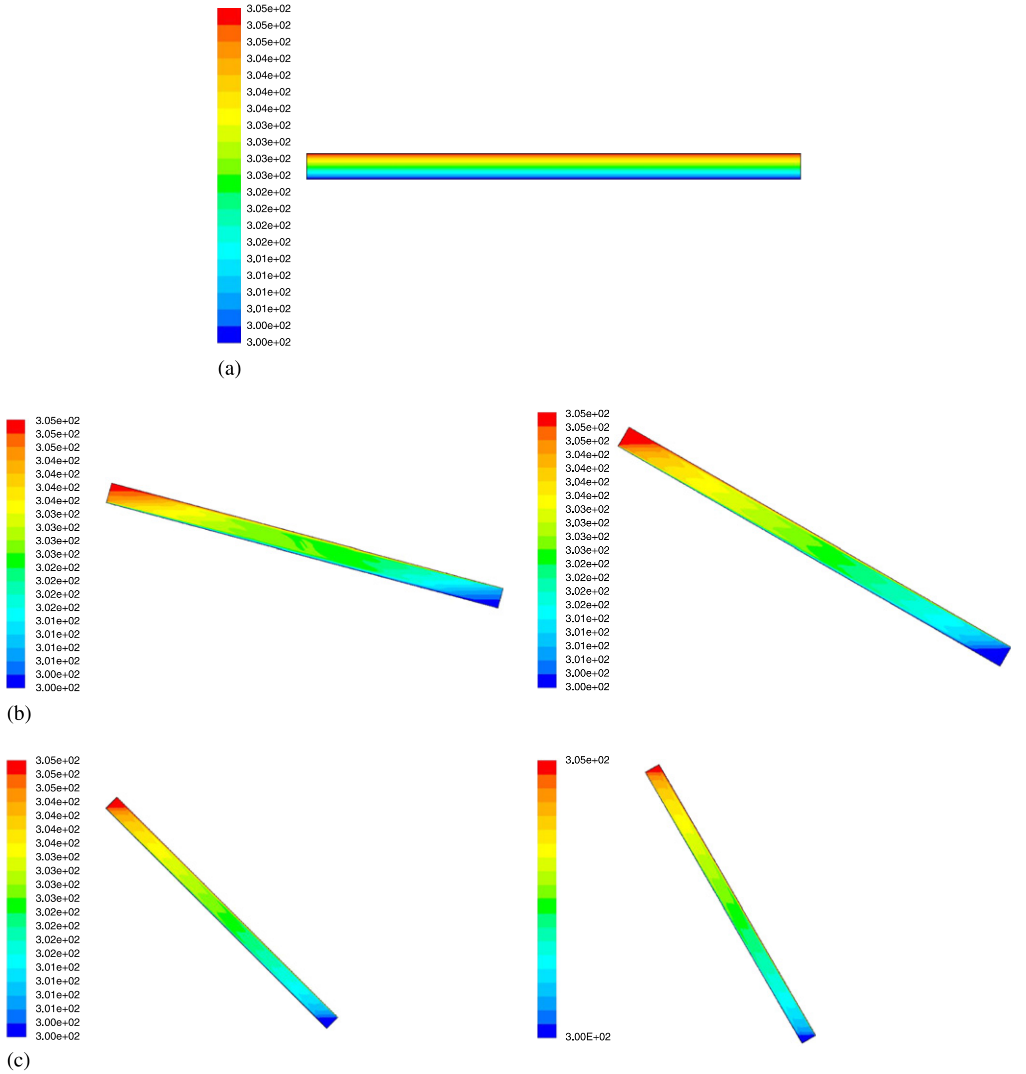

Fig. 19. Contours of temperature at (a) 0°, (b) 15° and 30° and (c) 45° and 75°.

7.5. Results from the CFD analysis

The results from 2D analysis of the water cavity and 3D analysis for the air cavity are shown in Figs. 18 and 19. The magnitude of the velocity inside the water cavity is seen to be increasing when moving toward the vertical orientation. Figs. 20a–d show the streak lines injected from the middle planes of the air cavity. These points are clearly indicated in Fig. 21. Initially, the strength of the rolls in both directions (longitudinal and lateral) is equal. As the inclination is increased, the rolls in the longitudinal direction pick up strength. The streak lines for flow at 75° indicate a single roll in the longitudinal direction. The flow at this point has passed the critical angle, and the lateral rolls have disappeared.

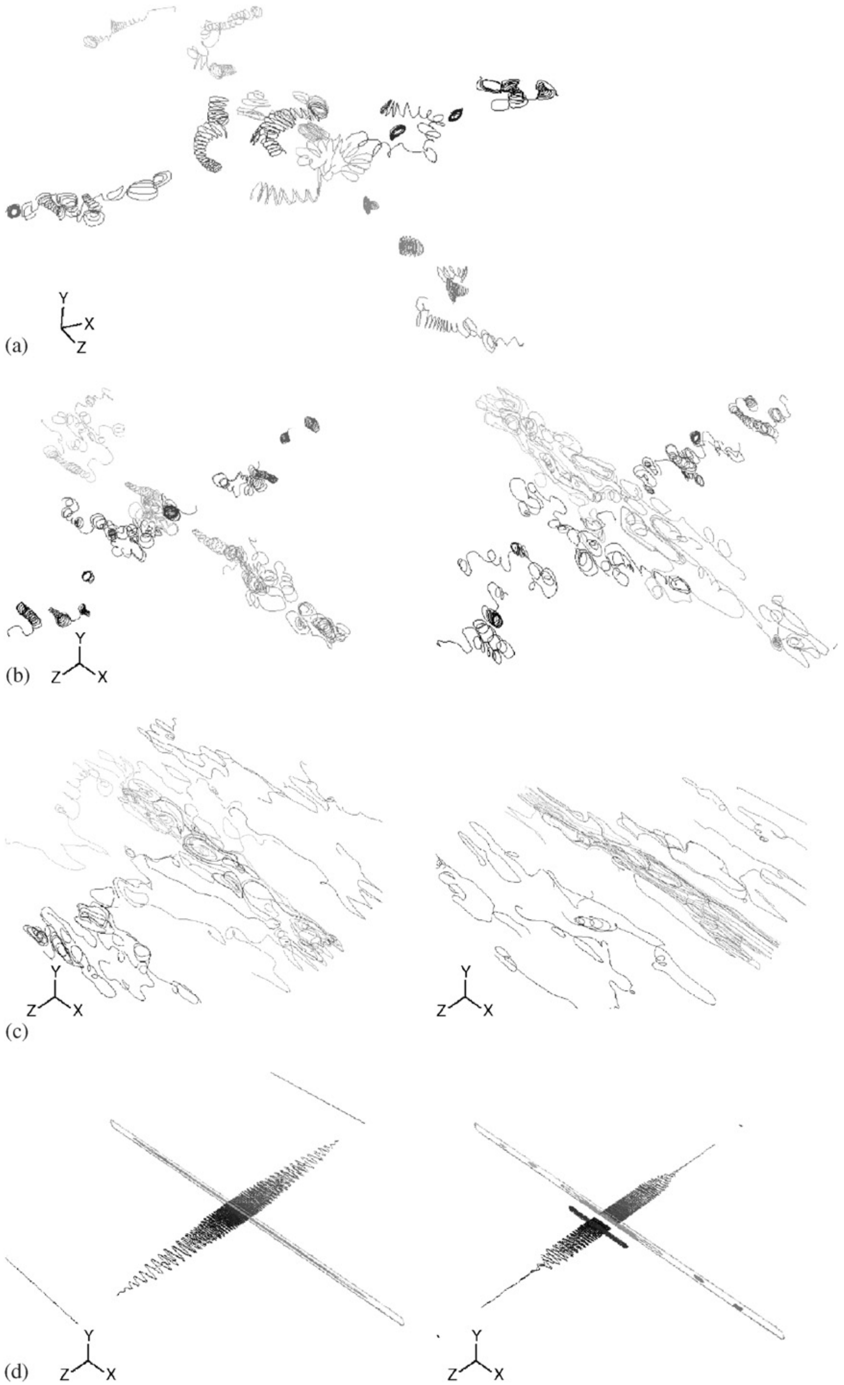

Fig. 20. (a) 3D CFD analysis of Elsherbiny's case. Streak lines indicate the 3D nature of the rolls which appear laterally as well as longitudinally. (b) 3D CFD Elsherbiny case study, streak lines for 15° and 30°. The strength of the longitudinal roll can be seen to be increasing. (c) 3D CFD Elsherbiny case study, streak lines 45° and 60°. (d) 3D CFD Elsherbiny case study, streak lines 75° and 90°. The flow has passed the critical angle regime and only a single cell in the longitudinal direction can be seen.

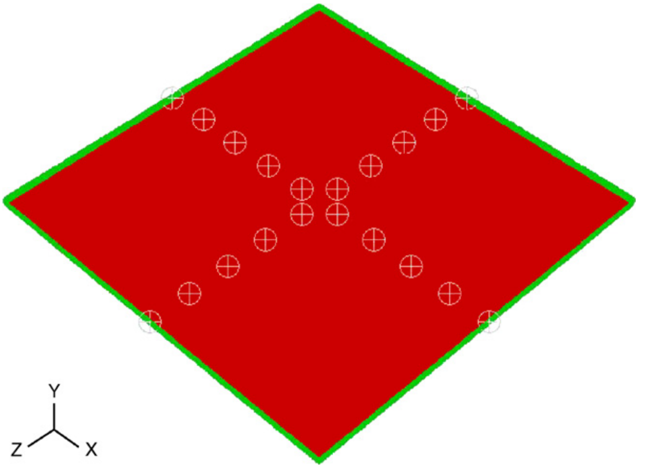

Fig. 21. The white marks indicate the injection points of the streak lines inside the air cavity. The angle for of inclination for the CFD analysis lies in the XY plane.

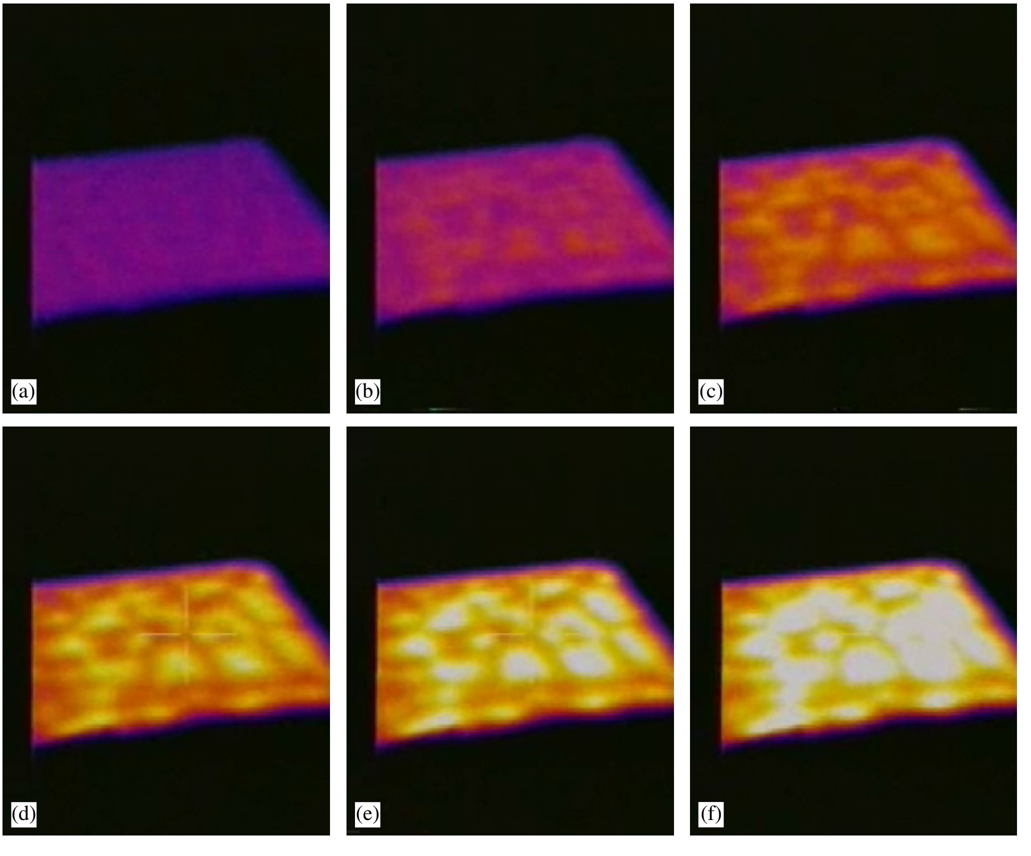

Fig. 22. Thermographic images of the air cavity at 0°: (a) 100, (b) 200, (c) 300, (d) 400, (e) 500 and (f) 600 s.

The results are very similar to the ones by finite difference formulation by Ozoe (Fig. 3). The finite difference results by Ozoe et al. were based on assumed domain size that would just slot-in the cell width. This was done to limit the computational domain. For CFD study, complete 3D domain was modeled ($1\,m \times 1m \times 0.035\,m$). The results found were very close to the results reported by Elsherbiny (Fig. 20).

8. Conclusions

The study of inclined cavity, although applicable to ICSSWH, has not been made use of in the designing or installing the device. It can be applied to both the air gap and the water tank, which are the only components that make up the ICSSWH. For the air cavity, due to high aspect ratio, the Benard convection cells prevail for nearly all practical angles of inclination of the heater. The common conclusion from the review of previous studies reveals that the behavior for large aspect ratios cavities is a decrease in Nusselt number till a minimum is reached when increasing the angle from 0°. This point of minimum heat transfer marks the critical angle where flow changes its pattern from complex longitudinal rolls to hydrodynamic circulation. On further increasing the inclination the Nusselt number climbs to a second maxima and thereafter exhibits a sinusoidal decline till it reaches a value of '1' at 180°.

The treatment of the water tank as a conventional inclined cavity was argued. It was, however, found that the trend for water cavity even with different boundary conditions remained similar to a conventional cavity for a transient simulation of 10 min.

It was also shown by processing 27-year irradiance data for Edinburgh that peak value irradiance falls at an angle of 35° rather than 49° as predicted by the general rule of thumb (0.9 times latitude). Albeit the contradiction, 49° still remains the optimal angle as it would thermally perform far better than the former. The combined effect of the air cavity and the water tank is the improvement of performance of the ICSSWH with the increase of angle of inclination. A 5–10° increase in the angle of inclination for particular latitude would improve the thermal performance of the heater.

Acknowledgements

The work of Nicolas Lambert of Polytechnique Nantes while his internship at the Applied Energy Group, Napier University is highly appreciated. The kind attention of Prof. K.G.T. Hollands is also acknowledged.

References

[1] Smyth M, Eames PC, Norton B. Integrated collector storage solar water heaters. Renew Sust Energy Rev, doi:10.1016/j.rser.2004.11.001.
[2] Duffie JA, Beckman WA. Solar energy thermal processes. New York: Wiley; 1974.
[3] Groenhout NK, Behnia M, Morrison GL. Experimental measurement of heat loss in an advanced solar collector. Exp Thermal Fluid Sci 2002;269:131–7.
[4] Buchberg H, Catton I, Edwards DK. Natural convection in enclosed spaces—a review of application to solar energy collection. J Heat Transfer Trans ASME C 1976;98(2).
[5] Muneer T. Effect of design parameters on performance of built-in storage solar water heater. Energy Conserv Manage 1985;25(3):277–81.

[6] Hawas MM, Muneer T. Year round performance of thermosyphon solar water heater in Benghazi. Energy Conserv Manage 1984;24(3):237–42.
[7] Muneer T, Hawas MM. Experimental study of the thermosyphonic and built-in storage type solar water heaters. In: Energex 84 conference, Regina, Canada, June 1984.
[8] Muneer T, Hawas MM, Khalifa Y. Experimental and analytical performance study of a thermosyphon water heater. Energy Conserv Manage 1983;23(2):119–24.
[9] Muneer T, Maubleu S, Asif M. Prospects of solar water heating for textile industry in Pakistan. Renew Sust Energy Rev, doi:10.1016/j.rser.2004.07.003.
[10] De Graaf JGA, Van der Held EFM. The relation between the heat transfer and convection phenomena in enclosed plane air layers. Appl Sci Res 1953;3:393–409.
[11] Dropkin D, Somerscales E. Heat transfer by natural convection in liquids confined by two parallel plates which are inclined at various angles with respect to horizontal. J Heat Transfer Trans ASME C 1965;87:74–84.
[12] Hart JE. Stability of the flow in a differentially heated inclined box. J Fluid Mech 1971;47:547–76.
[13] Elsherbiny SM, Raithby GD, Hollands KGT. Heat transfer by natural convection across vertical and incline air layers. Trans ASME J Heat Transfer 1982;104:96–102.
[14] Elsherbiny SM, Hollands KGT, Raithby GD. Nusselt number distribution in vertical and inclined air layers. J Heat Transfer 1983;105:406–8.
[15] Hamady FJ, Lloyd HR, Yang HQ, Yang KT. Study of local natural convection heat transfer in an inclined enclosure. Int J Heat Mass Transfer 1989;32:1697–708.
[16] Linthrost SJM, Schinkel WMM, Hoogendorn CJ. Flow structure with natural convection in inclined air filled enclosures. J Heat Transfer 1981;103:535–9.
[17] Yang HQ, Yang KT, Lloyd JD. Flow transition in laminar buoyant flow in three dimensional tilted rectangular enclosure. In: Proceedings of the international heat transfer conference, vol. 4, 1986.
[18] Zhong ZY, Yang KT, Llyod JR. Variable property natural convection in tilted enclosure with thermal radiation. Numer Methods Heat Transfer 1985;III:195–214.
[19] Ozoe H, Yamamoto K, Sayama H, Churchill SW. Natural circulation in an inclined rectangular channel heated on one side and cooled on the opposing side. Int J Heat Mass Transfer 1974;17:1209–17.
[20] Ozoe HK, Yamamoto H, Sayama H, Churchill SW. Natural circulation in an inclined rectangular channel at various aspect ratios and angles, experimental measurements. Int J Heat Mass Transfer 1975;18: 1425–31.
[21] Ozoe HK, Sayama H, Churchill SW. Natural convection in an inclined rectangular box heated from below. Three directional photography. Int J Heat Mass Transfer 1977;20(2):123–9.
[22] Ozoe H, Fujii K, Lior N, Churchill SW. Long rolls generated by natural convection in an inclined, rectangular enclosure. Int J Heat Mass Transfer 1983;26(10):1427–38.
[23] Bian W, Vasseur P, Bilgen E, Meng F. Effect of an electromagnetic field on natural convection in an inclined porous layer. Int J Heat Fluid Flow 1996;17(1):36–44.
[24] Adjlout L, Imine O, Azzi A, Belkadi M. Laminar natural convection in an inclined cavity with a wavy wall. Int J Heat Mass Transfer 2002;45(10):2141–52.
[25] Polat O, Bilgen E. Laminar natural convection in inclined open shallow cavities. Int J Thermal Sci 2002;41(4):360–8.
[26] Amaresh D, Manab Kumar D. Laminar natural convection in an inclined complicated cavity with spatially variable wall temperature. Int J Heat Mass Transfer 2005;48(18):3833–54.
[27] Kuyper RA, Van Der Meer ThH, Hoogendorn CJ, Henkes RAW. Numerical study of laminar and turbulent natural convection in an inclined square cavity. Int J Heat Mass Transfer 1992;36(11):2899–911.
[28] Elsherbiny SM. Free convection in inclined air layers heated from above. Int J Heat Mass Transfer 1996;39(18):3925–30.
[29] Hollands KGT, Konicek L. Experimental study of the stability of differentially heated inclined air layers. Int J Heat Mass Transfer 1973;16:1467–76.
[30] Hollands KGT, Unny SE, Raithby GD, Konicek L. Free convective heat transfer across inclined air layers. Trans ASME 1976;98C:189.
[31] Catton I, Ayyaswamy PS, Clever RM. Natural convectional flow in a rectangular slot arbitrarily oriented with respect to the gravity vector. Int J Heat Mass Transfer 1974;17:173–84.
[32] Arnold JN, Catton I, Edwards DK. Experimental investigation of natural convection in inclined rectangular regions of differing aspect ratios. J Heat Transfer 1976;98:67–71.

[33] Schinkel WMM, Hoogendorn CJ. An interferometric study of local heat transfer by natural convection in inclined air filled enclosures. In: Proceedings of the sixth international heat transfer conference, Toronto, vol. 2, 1978. p. 287–92.
[34] Chen CJ, Talaie V. Finite analytic numerical solution of laminar natural convection in two dimensional inclined rectangular enclosures. In: ASME paper 85-HT-10. 1985.
[35] Soong CY, Tzeng PY, Chiang DC, Sheu TS. Numerical study on mode-transition of natural convection in differentially heated inclined enclosures. Int J Heat Transfer 1996;39(14):2869–82.
[36] Soong CY, Tzeng PY, Lloyd JD. Flow transition in laminar bouyant flow in a three-dimensional tilted rectangular enclosure. In: Proceedings of the international heat transfer conference, vol. 4, 1986.
[37] Yang Y. Laminar natural convective flow in inclined rectangular glazing cavities. CEERE, University of Massachusetts, Department of Mechanical Engineering and Industrial Engineering, January 2002.
[38] Clever RM. Finite amplitude longitudinal convection rolls in an inclined layer. J Heat Transfer Trans ASME C 1973;95(3):407–8.
[39] Incropera FP, DeWitt DP. Fundamental of heat and mass transfer. New York: Wiley; 2002.
[40] Muneer T, Kubie J, Grassie T. Heat transfer a problem solving approach. London: Taylor & Francis; 2003.
[41] Dubois M, Berge P. Experimental study of the velocity field in a Rayleigh–Benard convection. J Fluid Mech 1978;85:641–53.
[42] Oertel Jr H. Three-dimensional convection within rectangular boxes. ASME HTD 1980;8:11–6
H. Oertel Jr. Thermische Zellularkonvection, Habilitationschrift. Universitat Karlsruhe, 1979.
[43] Hottel HC. Performance of flat-plate solar energy collectors. Space heating with solar energy. In: Proceedings of a course symposium. Cambridge: MIT Press; 1954. p. 58–71.
[44] Fluent 6.2 Documentation, User's Guide 2005, Fluent Inc.
[45] Zhai Z, Chen (Yan) C. Numerical determination and treatment of convective heat transfer coefficient in coupled building energy simulation. Build Environ 2004;39:1001–9.
[46] Technical Report. Modeling natural convection in a glazing cavity and predicting transition limits for multicellular flow from simulations on fluent. Bhaskar Adusumalli, August 2003, Technical Report, CEERE, University of Massachusetts.